symmetry

IMPACT FACTOR 2.940

CITESCORE 4.3

Article

Weak Gravitational Lensing around Bardeen Black Hole with a String Cloud in the Presence of Plasma

Farruh Atamurotov, Husan Alibekov, Ahmadjon Abdujabbarov, Ghulam Mustafa and Mersaid M. Aripov

Special Issue

Recent Progress of Black Holes Physics

Edited by

Dr. Ali Övgün

MDPI

https://doi.org/10.3390/sym15040848

symmetry

MDPI

Article

Weak Gravitational Lensing around Bardeen Black Hole with a String Cloud in the Presence of Plasma

Farruh Atamurotov [1,2,3,4,*], Husan Alibekov [5], Ahmadjon Abdujabbarov [4,5,6,7,8], Ghulam Mustafa [9,*] and Mersaid M. Aripov [10]

1 School of Mathematics and Natural Sciences, New Uzbekistan University, Mustaqillik Ave. 54, Tashkent 100007, Uzbekistan
2 College of Engineering, Akfa University, Milliy Bog' Street 264, Tashkent 111221, Uzbekistan
3 School of Computer and Information Engineering, Inha University in Tashkent, Ziyolilar 9, Tashkent 100170, Uzbekistan
4 Physics Faculty, National University of Uzbekistan, Tashkent 100174, Uzbekistan
5 Ulugh Beg Astronomical Institute, Astronomy St. 33, Tashkent 100052, Uzbekistan
6 Tashkent Institute of Irrigation and Agricultural Mechanization Engineers, Kori Niyoziy 39, Tashkent 100000, Uzbekistan
7 Institute of Nuclear Physics, Tashkent 100214, Uzbekistan
8 Power Engineering Faculty, Tashkent State Technical University, Tashkent 100095, Uzbekistan
9 Department of Physics, Zhejiang Normal University, Jinhua 321004, China
10 Applied Mathematics and Intelligent Technologies Faculty, National University of Uzbekistan, Tashkent 100174, Uzbekistan
* Correspondence: atamurotov@yahoo.com (F.A.); gmustafa3828@gmail.com (G.M.)

Abstract: The effect of spacetime curvature on optical properties may provide an opportunity to suggest new tests for gravity theories. In this paper, we investigated gravitational weak lensing around a Bardeen black hole with the string clouds parameter. First, we examined the horizon structure in the presence of string clouds around the gravitational compact object defined by Bardeen spacetime. The effect of gravitational weak lensing in a plasma medium is also discussed. According to the findings, the influence of the string cloud parameter on the circular orbits of a light ray around the black hole is greater than that in the Schwarzschild case, while the influence of the charge is reversed. The deflection angle of light rays in weak lensing is also used to study how much the image is magnified.

Keywords: weak gravitational lensing; black hole; Bardeen gravity; string cloud

Citation: Atamurotov, F.; Alibekov, H.; Abdujabbarov, A.; Mustafa, G.; Aripov, M.M. Weak Gravitational Lensing around Bardeen Black Hole with a String Cloud in the Presence of Plasma. *Symmetry* **2023**, *15*, 848. https://doi.org/10.3390/sym15040848

Academic Editor: Markus Büscher

Received: 2 March 2023
Revised: 28 March 2023
Accepted: 31 March 2023
Published: 2 April 2023

1. Introduction

In the modern study of gravitational fields, black holes (BHs) are regarded as one of the most distinctive features. Due to the strong gravitational influence, nothing can escape (either particles or radiations) from the event horizon of a BH, but it consumes everything in its vicinity. These thermodynamical entities not only characterize some outstanding classical insights but also improve our understanding of their quantum gravitational properties. Schwarzschild, Reissner–Nordström (RN), Kerr, and Kerr–Newmann are four well-known BH configurations that have a curvature singularity beyond their event horizons. Hawking radiations, also referred as thermal radiations, are emitted by BHs, and their emergence is supported by quantum mechanical considerations [1]. One of the major issues with the classical Maxwell theory is that a charge appears to have infinite self-energy at the charge location. While this discrepancy is easily addressed in quantum electrodynamics, it remains a challenge in classical electrodynamics. Born and Infeld created a unique Lagrangian to address this problem [2] in order to resolve it. More research has been conducted on other nonlinear electrodynamic fields than Born–Infeld nonlinear electrodynamics, including the logarithmic, exponential, and power law Maxwell

fields [3–5]. The black hole solution put forth by James Bardeen [6] was groundbreaking since it does not involve a curvature singularity, although there are currently many different kinds of black hole solutions available. The model was initially without a source, but after a few decades, Ayon-Beato and Garcia [7] provided a self-gravitating magnetic charge that was characterized by nonlinear electrodynamics [2], and this made it a precise solution of Einstein's equations. Nonlinear electrodynamics was shown to allow for the construction of a regular black hole [8], and as a result, we now have solutions that use electric charge as a source [9,10]. It is worth mentioning that the region where the weak energy condition is violated by any conventional black hole (including Bardeen black holes) is always protected by the Cauchy horizon [11]. The literature has various works about the Bardeen black hole. Eiroa and Sendra [12] investigated the gravitational lensing of a normal black hole. Zhou et al. [13] investigated the geodesic structure of test particles in the vicinity of the Bardeen black hole. Moreno and Sarbach [14] discussed gravitational and electromagnetic stability. Sharif and Javed [15] presented quantum corrections for the Bardeen black hole. Recently, Accretion disc properties, strong gravitational lensing, and Quasinormal modes of charged Naked singularity spacetime metric have been studied in detail in [16–18].

The most frequently mentioned candidate for "the final theory" is the string theory. The Universe is viewed as a collection of stretched objects rather than pointlike particles on it. A one-dimensional continuum string object is a promising candidate under the current scenario. M. Gürses and F. Gürsey [19] originally developed the string equation of motion in General Relativity, then demonstrated [20] that a fluid determined by this equation may describe the interior of a Kerr–Schild metric. An extension of the relativistic "dust cloud" model for a perfect fluid was later developed by J. Stachel [21]. As so, Letelier [22] solved Einstein's equations for clouds of strings and applied the result to the construction of a model of a star. As a result, many additional studies in the literature have interpreted string clouds to be fluids that serve as a background for black holes, whether charged or not. Hawking temperature, entropy, heat capacity, and Helmholtz free energy are computed and studied in the Einstein-Gauss-Bonnet gravity with a string cloud field by Herscovich and Richarte [23]. Another study [24] calculated quasinormal modes for a scalar field in such spacetime, emphasizing the function of the parameter associated with the clouds of strings. Ghosh and his coauthors Papnoi and Maharaj [25] found first- to third-order solutions of $D \geq 4$ dimensions and considered thermodynamic stability. Further, Ghosh and Maharaj, in another study [26], generalized the solution to N dimensions, evaluated the energy conditions, and studied the role of clouds of strings in the structure of the event horizon. Recently, Mustafa and his coauthors [27] discussed the shadow of the Schwarzschild BH in the background of the string cloud parameter and the quintessence parameter. Further, they extended their investigation in another study [28,29] to check the effect of charge within string cloud and the quintessence parameters.

It is necessary to mention that any novel approach or theory needs to be consistent with previous observations and pass the experimental tests. The optical properties, particularly light propagation in a curved background, can be used to test metric theories of gravity. In addition, the observation of the shadow by the EHT collaboration has compelled scientists to verify the modified theories of gravity using optical features of spacetime [30–32]. Light propagation in curved spacetime will be influenced by curvature due to strong gravity. The viewer may detect the black spot on the celestial plane as a result of photons captured by the central black hole. This black spot is known as a black hole shadow, and Synge [33] was the first to suggest this phenomena, later developed by Luminet [34] and Bardeen [35]. Several authors [36–56] have conducted substantial research on the black hole shadow. Various authors [57–69] have also thoroughly examined the impact of strong gravitational lensing caused by light deflection owing to spacetime curvature. On the other hand, the light propagation is sensitive to the plasma surrounding a compact gravitating object (for review see, e.g., [70–76]). The impact of different plasma topologies on light propagation have been investigated in [77–87].

The paper is formatted as follows: the features of a spacetime metric in Bardeen spacetime with a cloud of string parameter are defined in Section 2. The influence of plasma on gravitational weak lensing is discussed in more detail in Section 3. In Section 4, the magnification of an image in plasma medium is examined by utilizing the gravitational weak lensing phenomenon in Bardeen spacetime with the string cloud parameter a. Finally, in Section 5, we present the final outcomes on the deflection angle of light rays as well as magnifications.

2. Bardeen Spacetime with a Cloud of Strings

If we consider a spacetime pervaded by clouds of strings, we can construct a Bardeen solution from general relativity minimally connected to nonlinear electrodynamics and the cloud of strings by the following action of gravity

$$S = \int d^4x\sqrt{-g}[\mathcal{L}(F) + R] + S_C, \tag{1}$$

where g, R, $\mathcal{L}(F)$ are the metric determinant, curvature scalar, and the nonlinear general Lagrangian of electromagnetic theory, respectively. Further, $F = F^{\mu\nu}F_{\mu\nu}/4$ and S_C represent the function of the scalar and the Nambu–Goto action describing the stringlike objects, given by [22]. For the current analysis, in the Boyer–Linquist coordinate system, we take into account the spherically symmetric black hole solution reported by the researchers in Ref. [88]

$$ds^2 = -f(r)dt^2 + \frac{1}{f(r)}dr^2 + r^2(d\theta^2 + \sin^2\theta d\varphi^2), \tag{2}$$

with

$$f(r) = 1 - a - \frac{2Mr^2}{\sqrt{(q^2 + r^2)^3}}, \tag{3}$$

where q is the electric charge, M is the black hole's mass, and a represents the string cloud parameter. Now, using a cloud of strings and Bardeen gravity, it is possible to examine the structure of a black hole's horizon. To investigate it, one must examine the properties of the lapse function of the metric by constraining $f(r) = 0$ in order to obtain the structure of the BH horizon. Figure 1 demonstrates how the horizon is changing with the change of the parameter a. One can easily see from Figure 1 that the horizon approaches the central object with an increase in the q/M parameter. On the other hand, the location of the horizon shifts further from the center with an increase in the parameter of string clouds a. Further, the BH's permitted range for the parameters a and q may be obtained, as seen in Figure 2. Using a cloud string under Bardeen gravity, we determined the existence of BH and non-BH zones and obtained the dependency of the border between them on the BH parameters a and q.

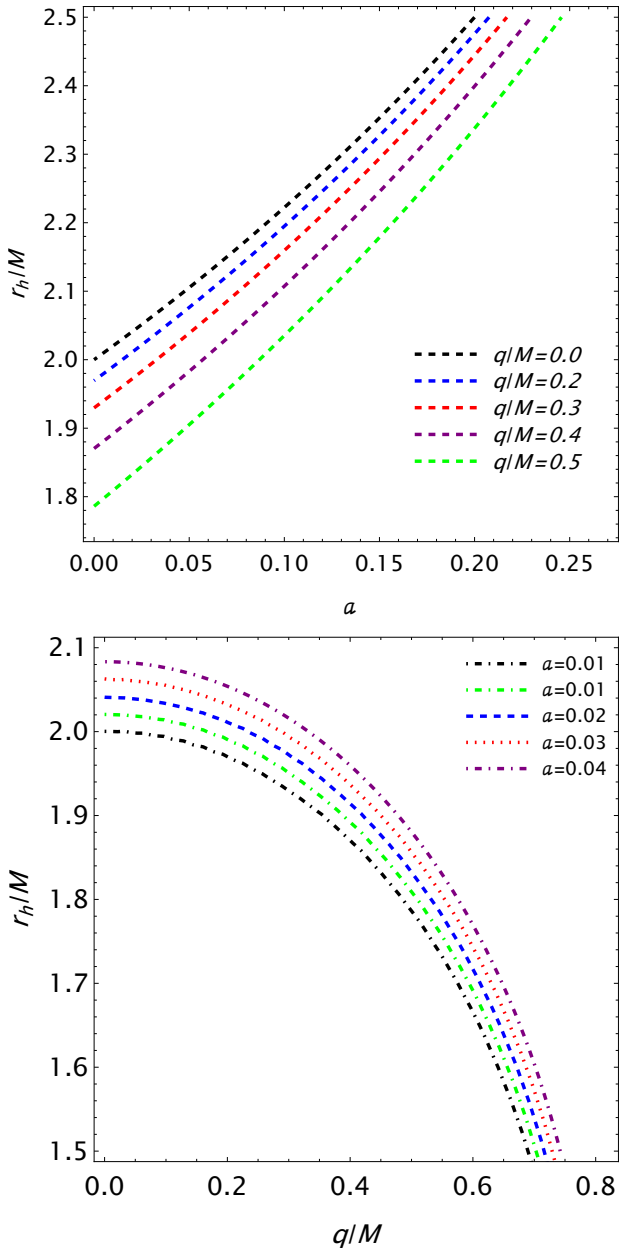

Figure 1. Plots of horizon radius versus the parameter a and q/M.

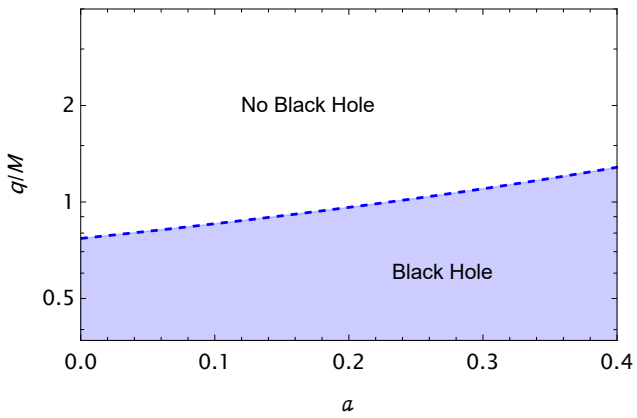

Figure 2. The separatrix line indicates the border corresponding to extremal black holes, which separates black holes from no black holes.

3. Weak Gravitational Lensing with Plasma

In the background of weak-field regime, the metric function (2) can be expressed as [77]:

$$g_{\alpha\beta} = \eta_{\alpha\beta} + h_{\alpha\beta}\,, \tag{4}$$

where the lapse function of Minkowski spacetime is represented by $\eta_{\alpha\beta}$, and the perturbed flat geometry is denoted with $h_{\alpha\beta}$, which is defined as [77]:

$$\begin{aligned} &\eta_{\alpha\beta} = \mathrm{diag}(-1,1,1,1),\\ &h_{\alpha\beta} \ll 1, \quad h_{\alpha\beta} \to 0 \quad \text{under} \quad x^i \to \infty\,,\\ &g^{\alpha\beta} = \eta^{\alpha\beta} - h^{\alpha\beta}, \quad h^{\alpha\beta} = h_{\alpha\beta}\,. \end{aligned} \tag{5}$$

Here, we may take into account how the plasma affects the deflection angle $\hat{\alpha}_k$ in a BH gravitationally weak field. It is possible to formulate the general equation for the deflection angle when plasma is present as [77,81]

$$\hat{\alpha}_i = \frac{1}{2}\int_{-\infty}^{\infty}\left(h_{33} + \frac{h_{00}\omega^2 - K_e N(x^i)}{\omega^2 - \omega_e^2}\right)_{,i} dz,\ i = 1,2 \tag{6}$$

where ω, ω_e, $K_e = 4\pi e^2/m_e$, and $N(x^i)$ denote the frequency of photon, frequency of the plasma, a real constant, and particle number density of plasma, respectively [77], and z is an axis for the motion of a photon in a curvature (see Figure 7). For the deflection angle, by considering Equations (5) and (6), the Equation (6) can be written as [77]:

$$\begin{aligned} \hat{\alpha}_b \;=\; & \frac{1}{2}\int_{-\infty}^{\infty}\frac{b}{r}\Big(\frac{dh_{33}}{dr} + \frac{1}{1-\omega_e^2/\omega^2}\frac{dh_{00}}{dr}\\ & - \frac{K_e}{\omega^2-\omega_e^2}\frac{dN}{dr}\Big)dz, \end{aligned} \tag{7}$$

where the impact parameter is denoted with b. It is interesting to mention that $\hat{\alpha}_b$ can be considered for both values (negative or positive) [77].

Far away from the BH, the line element for the weak-field region becomes (2)

$$\begin{aligned} ds^2 \;=\; & ds_0^2 + \left(a + \frac{R_s}{r} - \frac{3R_s q^2}{2r^3}\right)dt^2\\ & + \left(a + \frac{R_s}{r} - \frac{3R_s q^2}{2r^3}\right)dr^2, \end{aligned} \tag{8}$$

where $ds_0^2 = -dt^2 + dr^2 + r^2(d\theta^2 + \sin^2\theta d\phi^2)$. For convenience, a new notation, $R_s = 2M$, has been devised to represent the metric component of Minkowski spacetime geometry.

Rewriting the components $h_{\alpha\beta}$ in Cartesian coordinates allows one to study the deflection angle of light in the background of a plasma medium using Equation (10) as

$$\begin{aligned} h_{00} \;&=\; \left(a + \frac{R_s}{r} - \frac{3R_s q^2}{2r^3}\right),\\ h_{ik} \;&=\; \left(a + \frac{R_s}{r} - \frac{3R_s q^2}{2r^3}\right)n_i n_k,\\ h_{33} \;&=\; \left(a + \frac{R_s}{r} - \frac{3R_s q^2}{2r^3}\right)\cos^2\chi\,, \end{aligned} \tag{9}$$

where $\cos^2\chi = z^2/(b^2+z^2)$ and $r^2 = b^2 + z^2$ are introduced (see, e.g., [81]). The impact parameter b can be interpreted as the closest approach of the photons arround a BH.

The angle of light deflection with respect to b for a black hole in a plasma environment may be calculated using the calculation Equation (10) as

$$\hat{\alpha}_b = \frac{1}{2}\int_{-\infty}^{\infty}\frac{b}{r}\Big(\frac{dh_{33}}{dr}+\frac{1}{1-\omega_e^2/\omega^2}\frac{dh_{00}}{dr} - \frac{K_e}{\omega^2-\omega_e^2}\frac{dN}{dr}\Big)dz. \tag{10}$$

To simplify things, we may expand the formula for the deflection angle to read as [80]:

$$\hat{\alpha}_b = \hat{\alpha}_1 + \hat{\alpha}_2 + \hat{\alpha}_3, \tag{11}$$

with

$$\begin{aligned}\hat{\alpha}_1 &= \frac{1}{2}\int_{-\infty}^{\infty}\frac{b}{r}\frac{dh_{33}}{dr}dz,\\ \hat{\alpha}_2 &= \frac{1}{2}\int_{-\infty}^{\infty}\frac{b}{r}\Big(\frac{1}{1-\omega_e^2/\omega^2}\frac{dh_{00}}{dr}\Big)dz,\\ \hat{\alpha}_3 &= \frac{1}{2}\int_{-\infty}^{\infty}\frac{b}{r}\Big(-\frac{K_e}{\omega^2-\omega_e^2}\frac{dN}{dr}\Big)dz,\end{aligned} \tag{12}$$

where the notations $\hat{\alpha}_1$ represents the contribution of deflection angle due to gravitational field, $\hat{\alpha}_2$ is uniform plasma, and $\hat{\alpha}_3$ denotes the non-uniform plasma. In this research, we employ Equations (11) and (12) to investigate the effect of plasma on the deflection angle produced by gravitational weak lensing. Following this introduction, we will break down each scenario and examine it separately.

3.1. Uniform Plasma with $\omega_e^2 = const$

In this section, we determine the angular deflection of light rays surrounding BH within the influence of a uniform plasma medium by considering the Equation (11) as [80]:

$$\hat{\alpha}_{uni} = \hat{\alpha}_{uni1} + \hat{\alpha}_{uni2} + \hat{\alpha}_{uni3}, \tag{13}$$

where $\hat{\alpha}_{uni1}$ and $\hat{\alpha}_{uni2}$ can be accounted for as a portion of the deflection angle caused by a uniform plasma with gravity and $\hat{\alpha}_{uni3} = 0$ caused by the uniform plasma. By adjusting the value of the parameter a in the expressions (11)–(13), one can determine the angle of deflection of light beams around BH in a uniform plasma environment as follows.

$$\hat{\alpha}_{uni} = \Big(\frac{\pi a}{2}+\frac{R_s}{b}+\frac{R_s q^2}{b^3}\Big) + \Big(\frac{R_s}{b}-\frac{3R_s q^2}{b^3}\Big)\frac{\omega^2}{\omega^2-\omega_e^2}\,. \tag{14}$$

For a wide range of values of a, q, and ω_e/ω, the deflection angle of light beams around BH is shown to depend on the impact parameter b in Figure 3. The dependence of the deflection angle on plasma frequency ω_e/ω, charge q, and parameter a for fixed values of impact parameter is represented in the other three plots on the right of Figure 3. These graphs suggest that the existence of the plasma properties causes an increasing of the deflection angle of light beams around BH. Further, the angle at which light rays are bent increases when the parameter a is increased. By contrast, with the rise of parameter q, the value of the deflection angle decreases slightly until zero. With increasing impact of parameter b, the gravitational deflection angle approaches zero.

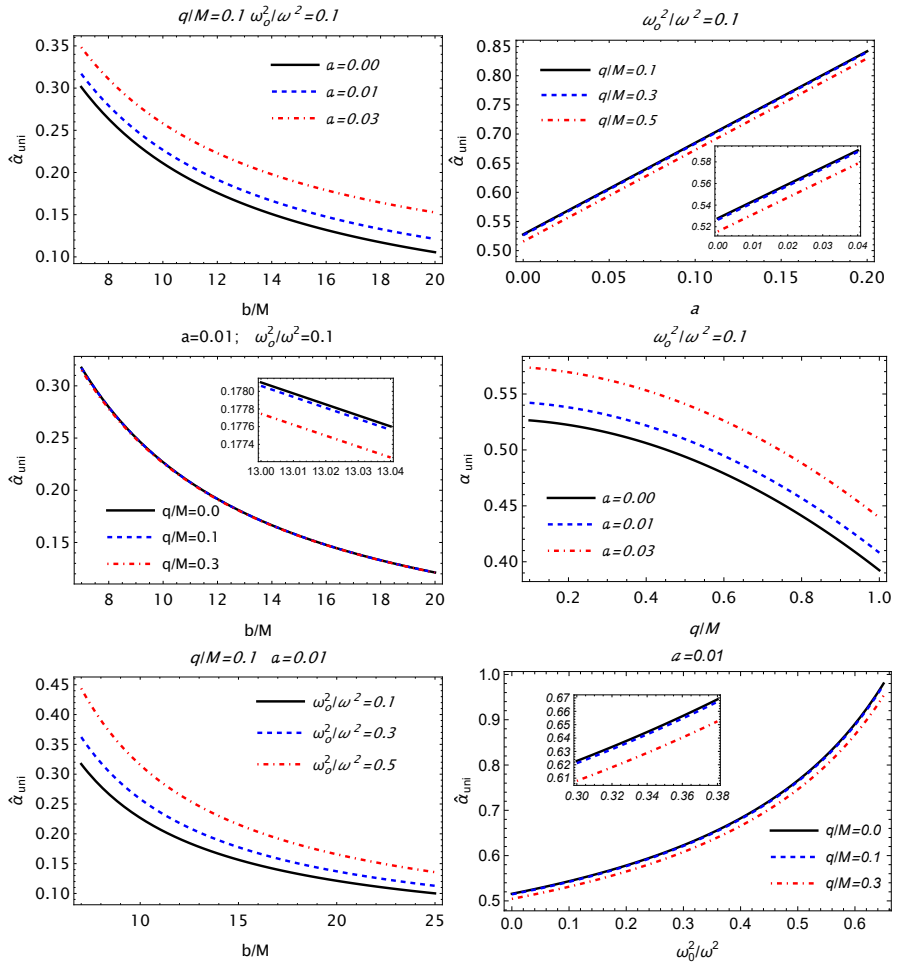

Figure 3. The dependence of the deflection angle $\hat{\alpha}_{uni}$ on the impact parameter b and parameter a, and magnetic charge q for different values of parameter a/M, plasma medium ω_e^2/ω^2, and magnetic charge q. The corresponding fixed parameter used is $b = 4$.

3.2. Non-Uniform Plasma with Singular Isothermal Sphere Medium

In the background of a non-uniform plasma with non-zero parameter a, we now investigate the angle by which light beams orbiting Bardeen BH are deflected. If we require a plasma distribution that is not perfectly uniform, we may use the Singular Isothermal Sphere (SIS) medium [77,81]. In the SIS medium, the plasma number density is represented as [77,81]

$$N(r) = \frac{\rho(r)}{km_p} \tag{15}$$

with

$$\rho(r) = \frac{\sigma_v^2}{2\pi r^2} \tag{16}$$

where the density of plasma is $\rho(r)$ and the velocity of dispersion is denoted with σ_v [77]. In this situation, the Equation (11) may be written as follows for the non-uniform plasma case: [80]:

$$\hat{\alpha}_{SIS} = \hat{\alpha}_{SIS1} + \hat{\alpha}_{SIS2} + \hat{\alpha}_{SIS3}\,, \tag{17}$$

with $\hat{\alpha}_{SIS1}$ describing the gravity part and $\hat{\alpha}_{SIS2}$ representing the plasma effects. Additionally, $\hat{\alpha}_{SIS3}$ is used to discuss the density part of the non-uniform plasma. By using

Equations (9), (11), and (17), in the presence of a cloud of string parameters and non-uniform plasma, we may be able to derive the equation for the bending of light rays around a Bardeen BH:

$$\begin{aligned}\hat{\alpha}_{SIS} &= \frac{\pi a}{2}+\frac{2R_s}{b}-\frac{2R_s q^2}{b^3}\\ &\quad+\frac{R_s^2\omega_c^2}{\pi b\omega^2}\left(1-\frac{2R_s}{3b^2}-\frac{9R_s q^2}{5b^4}\right)\end{aligned} \tag{18}$$

where the following notation has been inserted for convenience:

$$\omega_c^2 = \frac{\sigma_v^2 K_e}{2km_p R_s^2}. \tag{19}$$

The left panels of Figure 4 correspond to the three different plots illustrating the dependence of the deflection angle on the impact parameter for fixed values of charge q, the parameter a, and plasma frequency ω_c/ω. From these plots, one may easily see that the gravitational deflection angle tends to zero with the rise of the impact parameter b. The right panels of Figure 4 show that the value of the deflection angle relies on the change of charge q, non-uniform plasma case, and parameter a. These figures illustrate that the deflection angle of the light rays decreases in the presence of the charge parameter q, and that the opposite is true under the impact of a non-uniform plasma medium and parameter a.

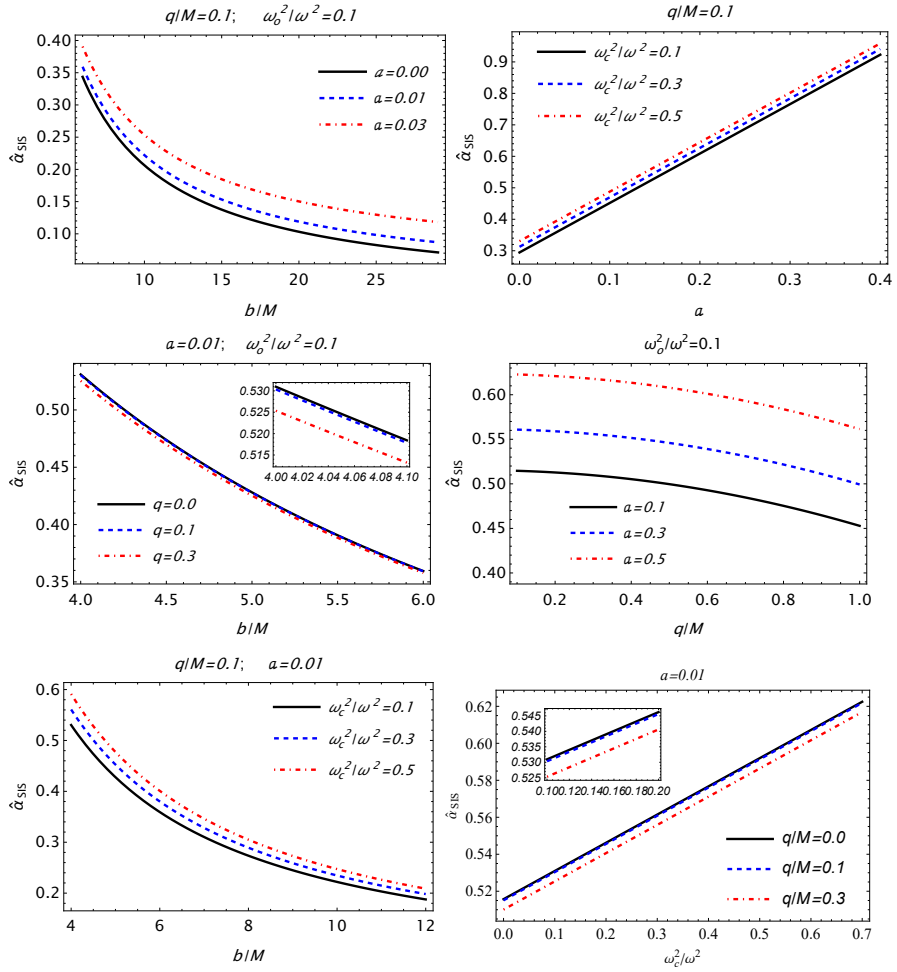

Figure 4. The effect of the impact parameter b, parameter a, and magnetic charge q on the deflection angle $\hat{\alpha}_{SIS}$ for different values of parameter a/M, plasma medium ω_c^2/ω^2, and magnetic charge q. The associated fixed parameter is $b = 4$.

3.3. Non-Singular Isothermal Gas Sphere

In order to provide a more realistic and physical context for the current research, we will now look at the mobility of photons using a non-singular isothermal sphere (NSIS). At its center, the gas cloud in the NSIS model has a finite core, and the density distribution is defined as [77,89]

$$\rho(r) = \frac{\sigma_v^2}{2\pi(r^2 + r_c^2)} = \frac{\rho_0}{(1 + \frac{r^2}{r_c^2})}, \quad \rho_0 = \frac{\sigma_v^2}{2\pi r_c^2}, \tag{20}$$

where the core radius is mentioned by r_c. Further, the plasma concentration (16) for NSIS is expressed as

$$N(r) = \frac{\sigma_v^2}{2\pi\kappa m_p(r^2 + r_c^2)}. \tag{21}$$

We compute the plasma frequency from Equations (20) and (21) as follows

$$\omega_e^2 = \frac{K_e\sigma_v^2}{2\pi\kappa m_p(r^2 + r_c^2)}. \tag{22}$$

Using the characteristics of the NSIS gravitational lens setup stated above, we can obtain the angle of deflection by photon deviation as follows:

$$\begin{aligned}\hat{\alpha}_{\mathrm{NSIS}} = &\left(\frac{\pi a}{2} + \frac{2R_s}{b} - \frac{2R_s q^2}{b^3}\right) + \frac{R_s^2\omega_c^2}{\omega^2}\left[\frac{R_s}{b\pi r_c^2}\right. \\ &- \frac{3b}{4(\sqrt{b^2 + r_c^2})^5}\frac{bR_s \arctan\frac{r_c}{\sqrt{b^2+r_c^2}}}{\pi r_c^3\sqrt{b^2 + r_c^2}} - \\ &\left.\frac{3R_s^2q^2}{\pi r_c^2}\left(\frac{3}{2br_c^3} + \frac{1}{b^3} - \frac{bR_s \arctan\frac{r_c}{\sqrt{b^2+r_c^2}}}{\pi r_c^3\sqrt{b^2 + r_c^2}}\right)\right].\end{aligned} \tag{23}$$

As before, we use the same graphical representation to show the NSIS's characteristics as they relate to photon velocity. The parameter ω_c^2/ω^2 is associated with the NSIS distribution here. When compared to the uniform plasma and SIS cases, it is clear from Figure 5 that the behavior of the impact parameter b, parameter α, magnetic charge q, and parameter ω_c^2/ω^2 cannot be distinguished from a specific point of view. However, one can at least identify the distribution that significantly affects the deflection angle. Figure 6 is a visual view of the $\hat{\alpha}_{\mathrm{uni}}$, $\hat{\alpha}_{\mathrm{SIS}}$, and $\hat{\alpha}_{\mathrm{NSIS}}$ as a function of the impact parameter and the coupling constant. The deflection is greatest when a homogeneous plasma medium surrounds the black hole, as can be seen. The following mathematical equation can be used to represent the outcome: $\hat{\alpha}_{\mathrm{uni}} > \hat{\alpha}_{\mathrm{SIS}} > \hat{\alpha}_{\mathrm{NSIS}}$.

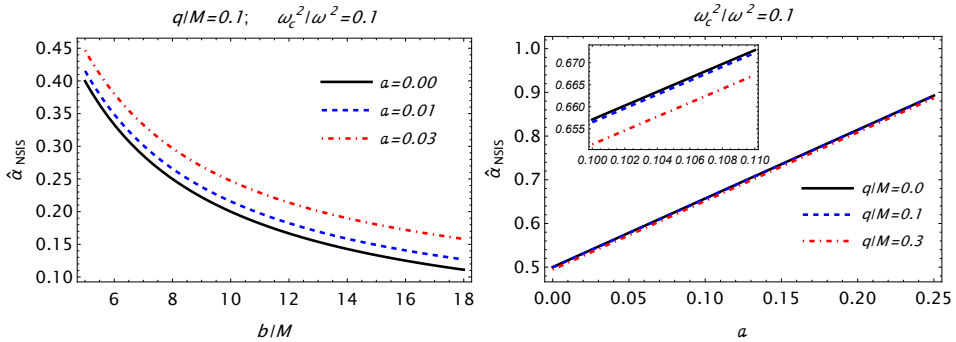

Figure 5. *Cont.*

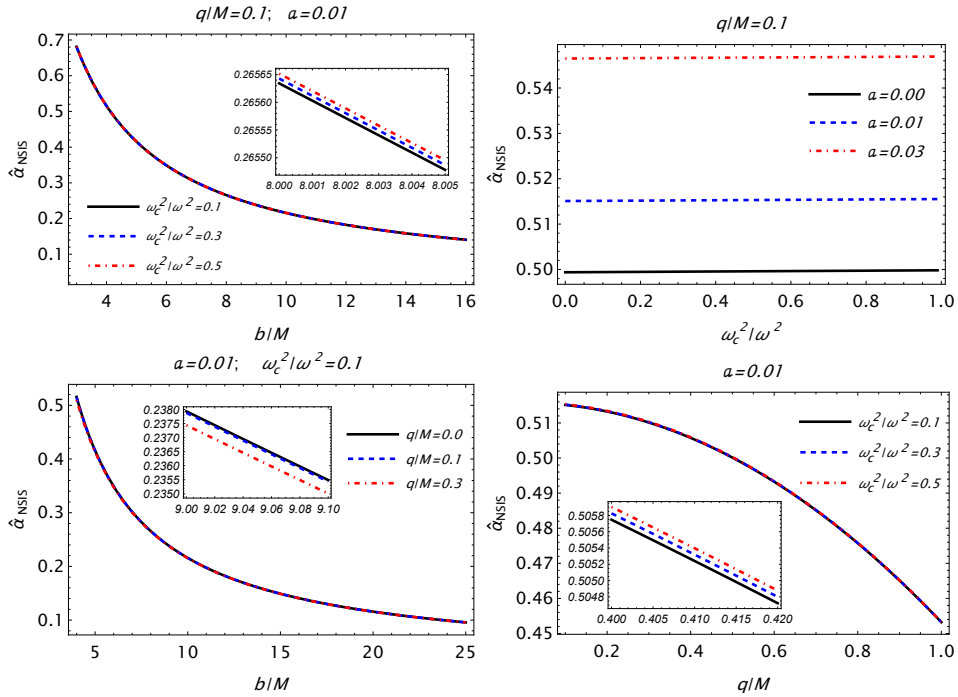

Figure 5. Deflection angle $\hat{\alpha}_{\mathrm{NSIS}}$ as a function of impact parameter b, plasma frequency $\frac{\omega_c^2}{\omega^2}$, and parameter a and magnetic charge q. The fixed parameters used are $b = 4$ and $r_c = 3$.

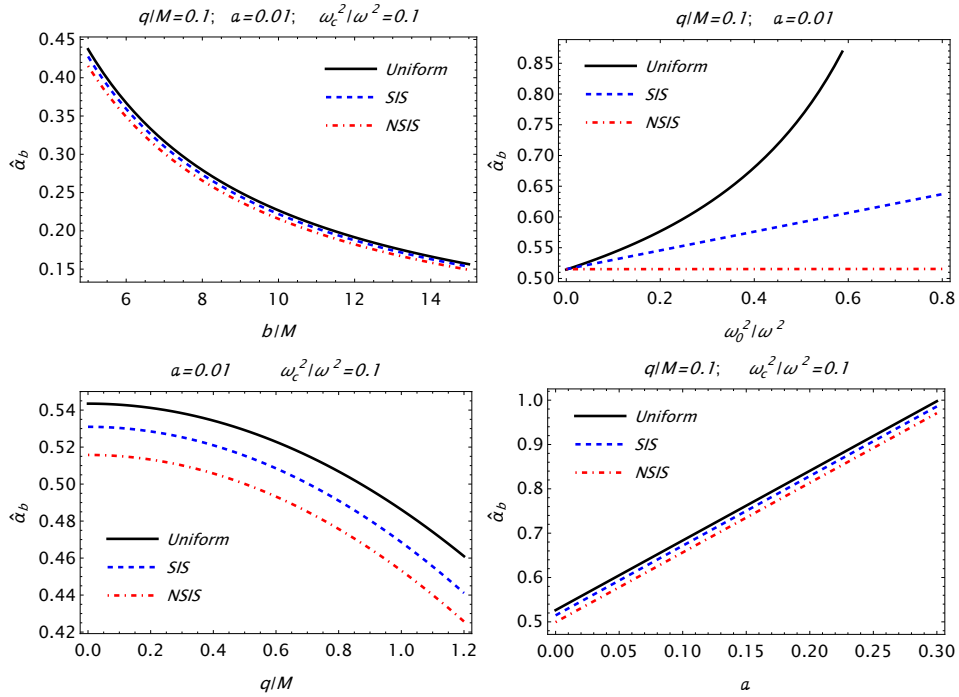

Figure 6. Plot of the deflection angle $\hat{\alpha}_b$ as a function of the impact parameter b, magnetic charge q, and parameter a. The corresponding fixed parameters used are $b = 4$ and $r_c = 3$.

4. Magnification of Image Source in the Presence of Plasma

We now use a lens equation of the form to understand more about magnification of an image source due to gravitational lensing in the context of a plasma (for a small deflection angle) [81,90]

$$\theta D_s = \hat{\alpha}_b D_{ds} + \beta D_s \,, \tag{24}$$

where D_s is the distances from observer to the distant source, and D_{ds} denotes the lens object (see Figure 7). The relation between the angle θ and the impact parameter b is represented by $b = D_d\theta$, where D_d denotes the observer distance from the lens object. By considering such relations, we can write Equation (24) as [68,81,90]

$$\beta = \theta - \frac{D_{ds}}{D_s}\frac{F(\theta)}{D_d}\frac{1}{\theta}, \tag{25}$$

with

$$F(\theta) = |\hat{\alpha}_b|b = |\hat{\alpha}_b(\theta)|D_d\theta.$$

Finally, using the above expressions, we can rewrite a lens equation for a small deflection angle in the following form [68]:

$$\beta = \theta - \frac{D_{ds}}{D_s}\hat{\alpha}_b\,. \tag{26}$$

The value of $\beta = 0$ is attained when the lens, observer, and source are all aligned along a single axis. In this case, the Einstein angle θ_E corresponds to the solution of the lens Equation (25) or (26), and the resulting image of the source takes the form of a so-called Einstein ring. For the Schwarzschild case, the deflection angle is $\hat{\alpha}_b = 2R_s/b$, and the radius of Einstein's ring is $R_E = D_d\theta_E$. Einstein's angle can be expressed as an instance of a Schwarzschild BH such as

$$\theta_{\mathrm{E}} = \sqrt{2R_E\frac{D_{ds}}{D_sD_d}}\,. \tag{27}$$

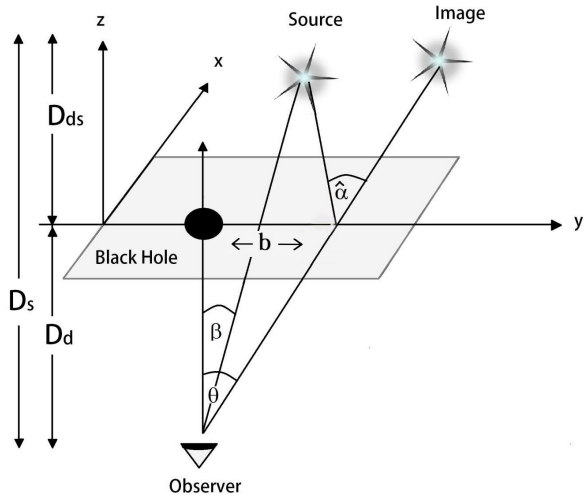

Figure 7. Schematic view of the gravitational lensing system (adopted from Ref. [81]).

We examine the source's image brightness magnification in depth to learn more about both the source and the lens object, which is directly connected to the observation. The following form can be used as a generic equation for determining the magnification of the picture source [77]:

$$\mu_\Sigma = \frac{I_{\mathrm{tot}}}{I_*} = \sum_k \left|\left(\frac{\theta_k}{\beta}\right)\left(\frac{d\theta_k}{d\beta}\right)\right|, \quad k = 1, 2, \ldots, s\,, \tag{28}$$

where I_{tot} and s denote increased brightness I_* and the total number of images of the source, respectively.

We now visualise the discussion of the effects of uniform and non-uniform plasma on the amplification of the picture source in the Bardeen spacetime metric by use of a cloud of string parameters.

4.1. Uniform Plasma with $\omega_e^2 =$ const

(θ_E^{pl}) is the Einstein angle in the background of uniform plasma with parameters q and a. From the Equations (14) and (25), one can obtain the following form of equation

$$(\theta_E^{pl})_{\rm uni} = \theta_{\rm E}\left(\frac{b}{2R_s}\hat{\alpha}_{uni}(b)\right)^{1/2}. \tag{29}$$

To determine the Einstein's angle, we use $b = D_d(\theta_E^{pl})_{\rm uni}$ in Equation (29) and then evalute the equation considering $(\theta_E^{pl})_{\rm uni}$. The analytical solution of the equation is very difficult. However, numerical computations may be used to determine the relationship between Einstein's angle and the BH and plasma properties.

From Equation (28), the term "magnification of the visual source" may be quickly understood as

$$\mu_{tot}^{pl} = \mu_+^{pl} + \mu_-^{pl} = \frac{x_{uni}^2+2}{x_{uni}\sqrt{x_{uni}^2+4}}, \tag{30}$$

where

$$x_{uni} = \frac{\beta}{(\theta_E^{pl})_{\rm uni}}. \tag{31}$$

The image source's magnifications are expressed as

$$\left(\mu_+^{pl}\right)_{\rm uni} = \frac{1}{4}\left(\frac{x_{uni}}{\sqrt{x_{uni}^2+4}} + \frac{\sqrt{x_{uni}^2+4}}{x_{uni}} + 2\right), \tag{32}$$

$$\left(\mu_-^{pl}\right)_{\rm uni} = \frac{1}{4}\left(\frac{x_{uni}}{\sqrt{x_{uni}^2+4}} + \frac{\sqrt{x_{uni}^2+4}}{x_{uni}} - 2\right). \tag{33}$$

One may graphically represent the relationship between the total magnification and the plasma parameter for various values of parameter a and magnetic charge q using Equation (30). This dependence is presented in Figure 8, and one can see that the total magnification of the image decreases due to the influence of magnetic charge q. Moreover, the total magnification increases with the increase of uniform plasma parameter and parameter a.

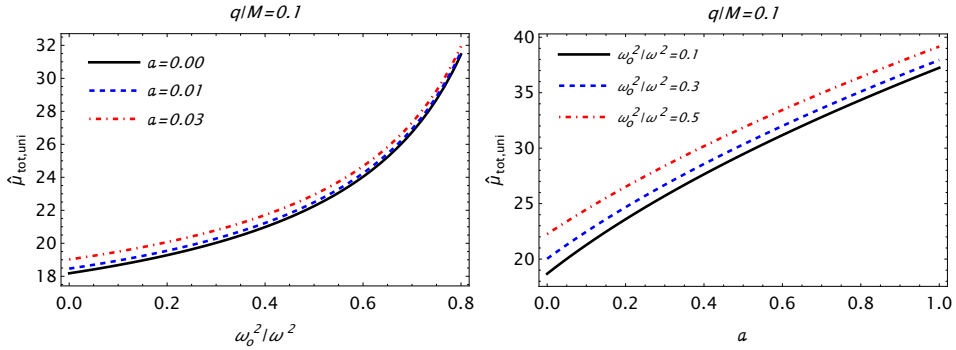

Figure 8. *Cont.*

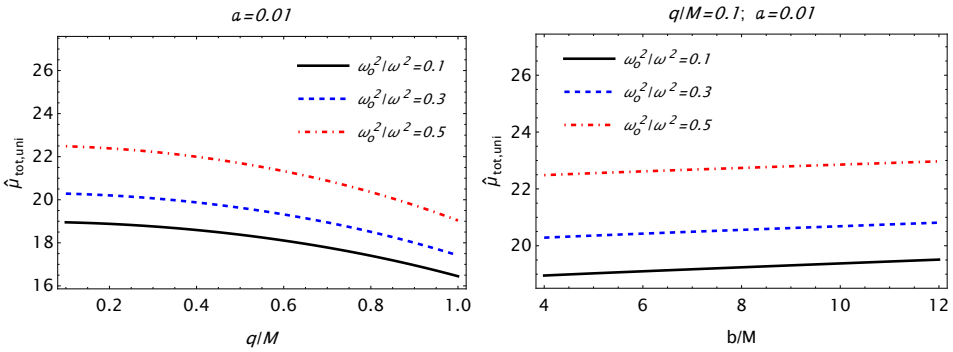

Figure 8. The total magnification of the image brightness in the presence of uniform plasma as a function of ω_c^2/ω^2, q, b, and a. The fixed parameters used are $R_s = 2$, $b = 3$, and $x_0 = 0.055$.

4.2. Non-Uniform Plasma with SIS Medium

In this subsection, we will discuss the overall source magnification when a non-uniform plasma medium surrounds the BH. By considering Equations (18) and (25), we calculate the mathematical expression for Einstein's ring by evaluating the equation

$$(\theta_E^{pl})_{\rm SIS} = \theta_{\rm E}\left(\frac{b}{2R_s}\hat{\alpha}_{SIS}(b)\right)^{1/2}. \tag{34}$$

The overall magnification of the picture source may be expressed as follows using the Equation (28) as

$$\begin{aligned}\left(\mu_{tot}^{pl}\right)_{\rm SIS} &= \left(\mu_{+}^{pl}\right)_{\rm SIS} + \left(\mu_{-}^{pl}\right)_{\rm SIS} \\ &= \frac{x_{SIS}^2+2}{x_{SIS}\sqrt{x_{SIS}^2+4}},\end{aligned} \tag{35}$$

where

$$\left(\mu_{+}^{pl}\right)_{\rm SIS} = \frac{1}{4}\left(\frac{x_{\rm SIS}}{\sqrt{x_{\rm SIS}^2+4}} + \frac{\sqrt{x_{\rm SIS}^2+4}}{x_{\rm SIS}} + 2\right), \tag{36}$$

$$\left(\mu_{-}^{pl}\right)_{\rm SIS} = \frac{1}{4}\left(\frac{x_{\rm SIS}}{\sqrt{x_{\rm SIS}^2+4}} + \frac{\sqrt{x_{\rm SIS}^2+4}}{x_{\rm SIS}} - 2\right), \tag{37}$$

$$x_{\rm SIS} = \frac{\beta}{(\theta_E^{pl})_{\rm SIS}}. \tag{38}$$

Figure 9 displays the relationship between magnetic charge q, the parameter a, and plasma properties and the overall magnification of the pictures of the source. It is clear from this relationship that the existence of the magnetic charge parameter causes the overall magnification to drop. However, the overall magnification grows when the non-uniform plasma parameter and the parameter a are both increased.

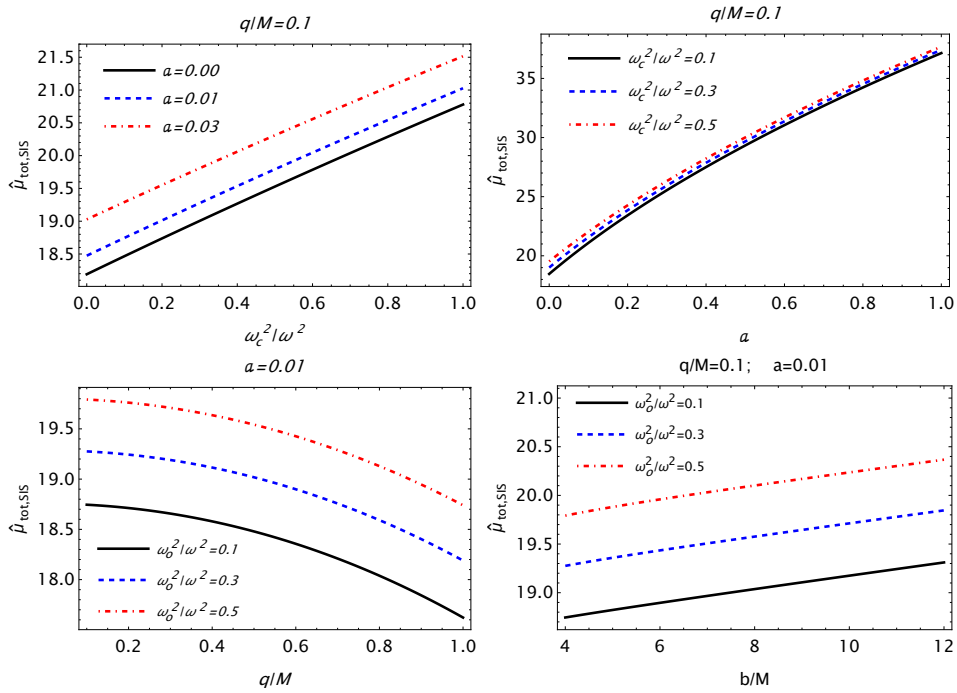

Figure 9. The total magnification of the image brightness in the presence of SIS as a function of ω_c^2/ω^2, q, b, and a. The fixed parameters used are $R_s = 2$, $b = 3$, and $x_0 = 0.055$.

5. Conclusions

This work carefully examines the impact of plasma (both uniform and non-uniform) on gravitational weak lensing for the Bardeen BH with a cloud of string. The following comments can be used to sum up the results:

- We analyzed the horizon radius for various values of the black hole in Bardeen gravity with a cloud string parameter a. The results show that the radius of horizon r_h is decreasing in the presence of parameter q, and the effect of string clouds is inverse.
- In the presence of the parameter a and magnetic charge q of the Bardeen spacetime metric with a cloud of a string field, the deflection angle of light beams around the BH decreases. In addition, with fixed values of the magnetic charge q and parameter a, the influence of uniform plasma on the gravitational weak deflection angle is also shown in Figure 3.
- As seen in Figure 4, the deflection angle of light rays around the compact object increases as the value of the parameter responsible for the non-uniform plasma medium increases.
- The deflection angle of a light beam around the BH is larger in the uniform case than in the non-uniform case, and this is true regardless of the values of the parameters a and q in the plasma (Figure 6).
- For various values of the parameter a and magnetic charge q in Bardeen spacetime in the presence of a cloud string field, we have explored the overall magnification of the image source caused by gravitational weak lensing. We have demonstrated that the magnetic charge q/M has an impact on the total magnification of the image but that the total magnification also increases with an increase in the parameter a (see Figures 8 and 9).
- Finally, we have investigated the total magnification's reliance on the plasma medium and found that it increases as the plasma medium's uniform and non-uniform properties are increased.

The observational data of the gravitational lensing in [91–94] may be further used to obtain constraints on the spacetime parameters and estimate the plasma characteristics.

Author Contributions: Conceptualization, F.A. and G.M.; Methodology, F.A. and A.A.; Software, H.A. and F.A.; Formal analysis, F.A., G.M. and M.M.A.; Investigation, H.A. and A.A.; Writing—original draft, A.A. and F.A.; Writing—review and editing, F.A., A.A., G.M. and M.M.A.; Visualization, H.A.; Supervision, F.A. All authors have read and agreed to the published version of the manuscript.

Funding: This research received no external funding.

Institutional Review Board Statement: Not applicable.

Informed Consent Statement: Not applicable.

Data Availability Statement: Data sharing not applicable—no new data generated.

Acknowledgments: This research is partly supported by Research Grant F-FA-2021-510 of the Uzbekistan Ministry for Innovative Development. AA thanks Silesian University in Opava for the hospitality during his visit. G. Mustafa is very thankful to Gao Xianlong from the Department of Physics, Zhejiang Normal University, for his kind support and help during this research. Further, G. Mustafa acknowledges Grant No. ZC304022919 to support his Postdoctoral Fellowship at Zhejiang Normal University.

Conflicts of Interest: The authors declare no conflict of interest.

References

1. Hawking, S.W. Black hole explosions? *Nature* **1974**, *248*, 30–31. [CrossRef]
2. Born, M.; Infeld, L. Foundations of the New Field Theory. *Proc. R. Soc. Lond. A* **1934**, *144*, 425–451. [CrossRef]
3. Hendi, S.H.; Panahiyan, S.; Eslam Panah, B. Geometrical method for thermal instability of nonlinearly charged BTZ Black Holes. *arXiv* **2015**, arXiv:1509.07014. [CrossRef]
4. Dehghani, M. Thermodynamics of (2 + 1)-dimensional charged black holes with power-law Maxwell field. *Phys. Rev. D* **2016**, *94*, 104071. [CrossRef]
5. Dehghani, M.; Hamidi, S.F. Thermal stability analysis of nonlinearly charged asymptotic AdS black hole solutions. *Phys. Rev. D* **2017**, *96*, 044025. [CrossRef]
6. Bardeen, J.M. Non-singular general-relativistic gravitational collapse. In Proceedings of the International Conference GR5, Tbilisi, Georgia, 9–16 September 1968; p. 174.
7. Ayón-Beato, E.; García, A. The Bardeen model as a nonlinear magnetic monopole. *Phys. Lett. B* **2000**, *493*, 149–152. [CrossRef]
8. Rodrigues, M.E.; Junior, E.L.B.; Silva, M.V.d.S. Using dominant and weak energy conditions for build new classe of regular black holes. *JCAP* **2018**, *2018*, 59. [CrossRef]
9. Dymnikova, I. Regular electrically charged vacuum structures with de Sitter centre in nonlinear electrodynamics coupled to general relativity. *Class. Quantum Gravity* **2004**, *21*, 4417–4428. [CrossRef]
10. Rodrigues, M.E.; Silva, M.V.d.S. Bardeen regular black hole with an electric source. *JCAP* **2018**, *2018*, 025. [CrossRef]
11. Bambi, C.; Modesto, L. Rotating regular black holes. *Phys. Lett. B* **2013**, *721*, 329–334. [CrossRef]
12. Eiroa, E.F.; Sendra, C.M. Gravitational lensing by a regular black hole. *Class. Quantum Gravity* **2011**, *28*, 085008. [CrossRef]
13. Zhou, S.; Chen, J.; Wang, Y. Geodesic Structure of Test Particle in Bardeen Spacetime. *Int. J. Mod. Phys. D* **2012**, *21*, 1250077. [CrossRef]
14. Moreno, C.; Sarbach, O. Stability properties of black holes in self-gravitating nonlinear electrodynamics. *Phys. Rev. D* **2003**, *67*, 024028. [CrossRef]
15. Sharif, M.; Javed, W. Quantum Corrections for a Bardeen Regular Black Hole. *J. Korean Phys. Soc.* **2010**, *57*, 217. [CrossRef]
16. Chirenti, C.; Saa, A.; Skákala, J. Quasinormal modes for the scattering on a naked Reissner-Nordström singularity. *Phys. Rev. D* **2012**, *86*, 124008. [CrossRef]
17. Joshi, P.S.; Malafarina, D.; Narayan, R. Distinguishing black holes from naked singularities through their accretion disc properties. *Class. Quantum Gravity* **2014**, *31*, 015002. [CrossRef]
18. Tsukamoto, N. Gravitational lensing by a photon sphere in a Reissner-Nordström naked singularity spacetime in strong deflection limits. *Phys. Rev. D* **2021**, *104*, 124016. [CrossRef]
19. Gürses, M.; Gürsey, F. Derivation of the string equation of motion in general relativity. *Phys. Rev. D* **1975**, *11*, 967–969. [CrossRef]
20. Gürses, M.; Gürsey, F. Lorentz covariant treatment of the Kerr-Schild geometry. *J. Math. Phys.* **1975**, *16*, 2385–2390. [CrossRef]
21. Stachel, J. String matter: Perfect dust and hydrodynamics. In Proceedings of the General Relativity and Gravitation 1977, Waterloo, NSW, Canada, 7–13 August 1977; p. 324.
22. Letelier, P.S. Clouds of strings in general relativity. *Phys. Rev. D* **1979**, *20*, 1294–1302. [CrossRef]
23. Herscovich, E.; Richarte, M.G. Black holes in Einstein-Gauss-Bonnet gravity with a string cloud background. *Phys. Lett. B* **2010**, *689*, 192–200. [CrossRef]
24. Graça, J.P.M.; Salako, G.I.; Bezerra, V.B. Quasinormal modes of a black hole with a cloud of strings in Einstein-Gauss-Bonnet gravity. *Int. J. Mod. Phys. D* **2017**, *26*, 1750113. [CrossRef]
25. Ghosh, S.G.; Papnoi, U.; Maharaj, S.D. Cloud of strings in third order Lovelock gravity. *Phys. Rev. D* **2014**, *90*, 044068. [CrossRef]

26. Ghosh, S.G.; Maharaj, S.D. Cloud of strings for radiating black holes in Lovelock gravity. *Phys. Rev. D* **2014**, *89*, 084027. [CrossRef]
27. Mustafa, G.; Atamurotov, F.; Hussain, I.; Shaymatov, S.; Övgün, A. Shadows and gravitational weak lensing by the Schwarzschild black hole in the string cloud background with quintessential field. *Chin. Phys. C* **2022**, *46*, 125107. [CrossRef]
28. Atamurotov, F.; Hussain, I.; Mustafa, G.; Övgün, A. Weak deflection angle and shadow cast by the charged-Kiselev black hole with cloud of strings in plasma. *Chin. Phys. C* **2023**, *47*, 025102. [CrossRef]
29. Atamurotov, F.; Hussain, I.; Mustafa, G.; Jusufi, K. Shadow and quasinormal modes of the Kerr-Newman-Kiselev-Letelier black hole. *Eur. Phys. J. C* **2022**, *82*, 831. [CrossRef]
30. Event Horizon Telescope Collaboration. First M87 Event Horizon Telescope Results. I. The Shadow of the Supermassive Black Hole. *Astrophys. J.* **2019**, *875*, L1. [CrossRef]
31. Event Horizon Telescope Collaboration. First M87 Event Horizon Telescope Results. VI. The Shadow and Mass of the Central Black Hole. *Astrophys. J.* **2019**, *875*, L6. [CrossRef]
32. Event Horizon Telescope Collaboration. First Sagittarius A* Event Horizon Telescope Results. I. The Shadow of the Supermassive Black Hole in the Center of the Milky Way. *Astrophys. J. Lett.* **2022**, *930*, L12. [CrossRef]
33. Synge, J.L. The escape of photons from gravitationally intense stars. *Mon. Not. Roy. Astron. Soc.* **1966**, *131*, 463. [CrossRef]
34. Luminet, J.P. Image of a spherical black hole with thin accretion disk. *Astron. Astrophys.* **1979**, *75*, 228–235.
35. Bardeen, J.M. Timelike and null geodesics in the Kerr metric. In *Black Holes*; Les Astres Occlus: Les Houches, France, 1973; pp. 215–239.
36. Falcke, H.; Melia, F.; Agol, E. Viewing the Shadow of the Black Hole at the Galactic Center. *Astrophys. J.* **2000**, *528*, L13–L16. [CrossRef] [PubMed]
37. Bambi, C.; Freese, K. Apparent shape of super-spinning black holes. *Phys. Rev. D.* **2009**, *79*, 043002. [CrossRef]
38. Hioki, K.; Maeda, K.I. Measurement of the Kerr spin parameter by observation of a compact object's shadow. *Phys. Rev. D* **2009**, *80*, 024042. [CrossRef]
39. Abdujabbarov, A.; Atamurotov, F.; Kucukakca, Y.; Ahmedov, B.; Camci, U. Shadow of Kerr-Taub-NUT black hole. *Astrophys. Space Sci.* **2013**, *344*, 429–435. [CrossRef]
40. Amarilla, L.; Eiroa, E.F. Shadow of a Kaluza-Klein rotating dilaton black hole. *Phys. Rev. D* **2013**, *87*, 044057. [CrossRef]
41. Atamurotov, F.; Abdujabbarov, A.; Ahmedov, B. Shadow of rotating non-Kerr black hole. *Phys. Rev. D* **2013**, *88*, 064004. [CrossRef]
42. Tsukamoto, N. Black hole shadow in an asymptotically flat, stationary, and axisymmetric spacetime: The Kerr-Newman and rotating regular black holes. *Phys. Rev. D.* **2018**, *97*, 064021. [CrossRef]
43. Ghasemi-Nodehi, M.; Azreg-Aïnou, M.; Jusufi, K.; Jamil, M. Shadow, quasinormal modes, and quasiperiodic oscillations of rotating Kaluza-Klein black holes. *Phys. Rev. D.* **2020**, *102*, 104032. [CrossRef]
44. EHT Collaboration. Constraints on black-hole charges with the 2017 EHT observations of M87*. *Phys. Rev. D.* **2021**, *103*, 104047. [CrossRef]
45. He, P.Z.; Fan, Q.Q.; Zhang, H.R.; Deng, J.B. Shadows of rotating Hayward-de Sitter black holes with astrometric observables. *Eur. Phys. J. C* **2020**, *80*, 1195. [CrossRef]
46. de Vries, A. The apparent shape of a rotating charged black hole, closed photon orbits and the bifurcation set A_4. *Class. Quantum Gravity* **2000**, *17*, 123–144. [CrossRef]
47. Abdujabbarov, A.A.; Rezzolla, L.; Ahmedov, B.J. A coordinate-independent characterization of a black hole shadow. *Mon. Not. R. Astron. Soc.* **2015**, *454*, 2423–2435. [CrossRef]
48. Grenzebach, A.; Perlick, V.; Lämmerzahl, C. Photon regions and shadows of Kerr-Newman-NUT black holes with a cosmological constant. *Phys. Rev. D* **2014**, *89*, 124004. [CrossRef]
49. Hou, X.; Xu, Z.; Wang, J. Rotating black hole shadow in perfect fluid dark matter. *J. Cosmol. Astropart. Phys.* **2018**, *2018*, 40. [CrossRef]
50. Perlick, V.; Tsupko, O.Y.; Bisnovatyi-Kogan, G.S. Black hole shadow in an expanding universe with a cosmological constant. *Phys. Rev. D.* **2018**, *97*, 104062. [CrossRef]
51. Cunha, P.V.P.; Eiró, N.A.; Herdeiro, C.A.R.; Lemos, J.P.S. Lensing and shadow of a black hole surrounded by a heavy accretion disk. *J. Cosmol. Astropart. Phys.* **2020**, *2020*, 035. [CrossRef]
52. Afrin, M.; Kumar, R.; Ghosh, S.G. Parameter estimation of hairy Kerr black holes from its shadow and constraints from M87*. *arXiv* **2021**, arXiv:2103.11417. [CrossRef]
53. Bambhaniya, P.; Dey, D.; Joshi, A.B.; Joshi, P.S.; Solanki, D.N.; Mehta, A. Shadows and negative precession in non-Kerr spacetime. *Phys. Rev. D.* **2021**, *103*, 084005. [CrossRef]
54. Cunha, P.V.; Herdeiro, C.A.; Kleihaus, B.; Kunz, J.; Radu, E. Shadows of Einstein–dilaton–Gauss–Bonnet black holes. *Phys. Let. B* **2017**, *768*, 373–379. [CrossRef]
55. Atamurotov, F.; Papnoi, U.; Jusufi, K. Shadow and deflection angle of charged rotating black hole surrounded by perfect fluid dark matter. *Class. Quantum Gravity* **2022**, *39*, 025014. [CrossRef]
56. Papnoi, U.; Atamurotov, F. Rotating charged black hole in 4 D Einstein-Gauss-Bonnet gravity: Photon motion and its shadow. *Phys. Dark Universe* **2022**, *35*, 100916. [CrossRef]
57. Bozza, V.; Capozziello, S.; Iovane, G.; Scarpetta, G. Strong field limit of black hole gravitational lensing. *Gen. Rel. Grav.* **2001**, *33*, 1535. [CrossRef]
58. Bozza, V. Gravitational lensing in the strong field limit. *Phys. Rev. D.* **2002**, *66*, 103001. [CrossRef]

59. Bozza, V.; Luca, F.D.; Scarpetta, G. Kerr black hole lensing for generic observers in the strong deflection limit. *Phys. Rev. D.* **2006**, *74*, 063001. [CrossRef]
60. Eiroa, E.F.; Torres, D.F. Strong field limit analysis of gravitational retro lensing. *Phys. Rev. D.* **2004**, *69*, 063004. [CrossRef]
61. Virbhadra, K.S.; Ellis, G.F.R. Schwarzschild black hole lensing. *Phys. Rev. D.* **2000**, *62*, 084003. [CrossRef]
62. Virbhadra, K.S.; Ellis, G.F.R. Gravitational lensing by naked singularities. *Phys. Rev. D.* **2002**, *65*, 103004. [CrossRef]
63. Virbhadra, K.S. Relativistic images of Schwarzschild black hole lensing. *Phys. Rev. D.* **2009**, *79*, 083004. [CrossRef]
64. Islam, S.U.; Kumar, R.; Ghosh, S.G. Gravitational lensing by black holes in the 4D Einstein-Gauss-Bonnet gravity. *J. Cosmol. Astropart. Phys.* **2020**, *2020*, 030. [CrossRef]
65. Lu, X.; Xie, Y. Weak and strong deflection gravitational lensing by a renormalization group improved Schwarzschild black hole. *Eur. Phys. J. C* **2019**, *79*, 1016. [CrossRef]
66. Wang, C.Y.; Shen, Y.F.; Xie, Y. Weak and strong deflection gravitational lensings by a charged Horndeski black hole. *JCAP* **2019**, *2019*, 022. [CrossRef]
67. Gao, Y.X.; Xie, Y. Gravitational lensing by hairy black holes in Einstein-scalar-Gauss-Bonnet theories. *Phys. Rev. D* **2021**, *103*, 043008. [CrossRef]
68. Bozza, V. Comparison of approximate gravitational lens equations and a proposal for an improved new one. *Phys. Rev. D* **2008**, *78*, 103005. [CrossRef]
69. Takizawa, K.; Ono, T.; Asada, H. Gravitational lens without asymptotic flatness: Its application to Weyl gravity. *Phys. Rev. D* **2020**, *102*, 064060. [CrossRef]
70. Perlick, V.; Tsupko, O.Y.; Bisnovatyi-Kogan, G.S. Influence of a plasma on the shadow of a spherically symmetric black hole. *Phys. Rev. D.* **2015**, *92*, 104031. [CrossRef]
71. Perlick, V.; Tsupko, O.Y. Light propagation in a plasma on Kerr spacetime: Separation of the Hamilton-Jacobi equation and calculation of the shadow. *Phys. Rev. D.* **2017**, *95*, 104003. [CrossRef]
72. Chowdhuri, A.; Bhattacharyya, A. Shadow analysis for rotating black holes in the presence of plasma for an expanding universe. *Phys. Rev. D* **2021**, *104*, 064039. [CrossRef]
73. Atamurotov, F.; Ahmedov, B.; Abdujabbarov, A. Optical properties of black holes in the presence of a plasma: The shadow. *Phys. Rev. D* **2015**, *92*, 084005. [CrossRef]
74. Atamurotov, F.; Jusufi, K.; Jamil, M.; Abdujabbarov, A.; Azreg-Aïnou, M. Axion-plasmon or magnetized plasma effect on an observable shadow and gravitational lensing of a Schwarzschild black hole. *Phys. Rev. D* **2021**, *104*, 064053. [CrossRef]
75. Babar, G.Z.; Babar, A.Z.; Atamurotov, F. Optical properties of Kerr–Newman spacetime in the presence of plasma. *Eur. Phys. J. C* **2020**, *80*, 761. [CrossRef]
76. Fathi, M.; Olivares, M.; Villanueva, J.R. Analytical study of light ray trajectories in Kerr spacetime in the presence of an inhomogeneous anisotropic plasma. *arXiv* **2021**, arXiv:2104.07721.
77. Bisnovatyi-Kogan, G.S.; Tsupko, O.Y. Gravitational lensing in a non-uniform plasma. *Mon. Not. R. Astron. Soc* **2010**, *404*, 1790–1800. [CrossRef]
78. Rogers, A. Frequency-dependent effects of gravitational lensing within plasma. *Mon. Not. R. Astron. Soc.* **2015**, *451*, 17. [CrossRef]
79. Atamurotov, F.; Abdujabbarov, A.; Han, W.B. Effect of plasma on gravitational lensing by a Schwarzschild black hole immersed in perfect fluid dark matter. *Phys. Rev. D* **2021**, *104*, 084015. [CrossRef]
80. Atamurotov, F.; Abdujabbarov, A.; Rayimbaev, J. Weak gravitational lensing Schwarzschild-MOG black hole in plasma. *Eur. Phys. J. C* **2021**, *81*, 118. [CrossRef]
81. Babar, G.Z.; Atamurotov, F.; Babar, A.Z. Gravitational lensing in 4-D Einstein-Gauss-Bonnet gravity in the presence of plasma. *Phys. Dark Universe* **2021**, *32*, 100798. [CrossRef]
82. Abdujabbarov, A.; Toshmatov, B.; Schee, J.; Stuchlík, Z.; Ahmedov, B. Gravitational lensing by regular black holes surrounded by plasma. *Int. J. Mod. Phys. D* **2017**, *26*, 1741011. [CrossRef]
83. Javed, W.; Hussain, I.; Övgün, A. Weak deflection angle of Kazakov-Solodukhin black hole in plasma medium using Gauss-Bonnet theorem and its greybody bonding. *Eur. Phys. J. Plus* **2022**, *137*, 148. [CrossRef]
84. Atamurotov, F.; Ghosh, S.G. Gravitational weak lensing by a naked singularity in plasma. *Eur. Phys. J. Plus* **2022**, *137*, 662. [CrossRef]
85. Ghaffarnejad, H.; niad, H. Weak Gravitational Lensing from Regular Bardeen Black Holes. *Int. J. Theor. Phys.* **2016**, *55*, 1492–1505. [CrossRef]
86. Atamurotov, F.; Alloqulov, M.; Abdujabbarov, A.; Ahmedov, B. Testing the Einstein-Æther gravity: particle dynamics and gravitational lensing. *Eur. Phys. J. Plus* **2022**, *137*, 634. [CrossRef]
87. Atamurotov, F.; Jamil, M.; Jusufi, K. Quantum effects on the black hole shadow and deflection angle in the presence of plasma. *Chin. Phys. C* **2023**, *47*, 035106. [CrossRef]
88. Rodrigues, M.E.; Vieira, H.A. Bardeen solution with a cloud of strings. *Phys. Rev. D* **2022**, *106*, 084015. [CrossRef]
89. Hinshaw, G.; Krauss, L.M. Gravitational Lensing by isothermal spheres with finite core radii: galaxies and dark matte. *Ap. J.* **1987**, *320*, 468. [CrossRef]
90. Morozova, V.S.; Ahmedov, B.J.; Tursunov, A.A. Gravitational lensing by a rotating massive object in a plasma. *Astrophys. Space Sci.* **2013**, *346*, 513–520. [CrossRef]
91. Wang, Y. Observational signatures of the weak lensing magnification of supernovae. *JCAP* **2005**, *2005*, 005. [CrossRef]

92. Gonzalez, E.J.; Foëx, G.; Nilo Castellón, J.L.; Domínguez Romero, M.J.; Alonso, M.V.; García Lambas, D.; Moreschi, O.; Gallo, E. Low X-ray luminosity galaxy clusters—III. Weak lensing mass determination at $0.18 < z < 0.70$. *MNRAS* **2015**, *452*, 2225–2235. [CrossRef]
93. Kalantari, Z.; Rahvar, S.; Ibrahim, A. Fermi-GBM Observation of GRB 090717034: χ^2 Test Confirms Evidence of Gravitational Lensing by a Supermassive Black Hole with a Million Solar Mass. *Astrophys. J.* **2022**, *934*, 106. [CrossRef]
94. Wen, D.; Kemball, A.J. Testing Primordial Black Hole Dark Matter with ALMA Observations of the Gravitational Lens B1422 + 231. *arXiv* **2022**, arXiv:2210.16444. [CrossRef]